

X-ray Hardness Variations as an Internal/External Shock Diagnostic

Nathaniel R. Butler^{1,2} and Daniel Kocevski²

ABSTRACT

The early, highly time-variable X-ray emission immediately following GRBs exhibits strong spectral variations that are unlike the temporally smoother emission which dominates after $t \sim 10^3$ s. The ratio of hard channel (1.3-10.0 keV) to soft channel (0.3-1.3 keV) counts in the Swift X-ray telescope provides a new measure delineating the end time of this emission. We define T_H as the time at which this transition takes place and measure for 59 events a range of transition times that span 10^2 s to 10^4 s, on average 5 times longer than the prompt T_{90} duration observed in the Gamma-ray band. It is very likely that the mysterious light curve plateau phase and the later powerlaw temporal evolution, both of which typically occur at times greater than T_H and hence exhibit very little hardness ratio evolution, are both produced by external shocking of the surrounding medium and not by the internal shocks thought responsible for the earlier emission. We use the apparent lack of spectral evolution to discriminate against proposed models for the plateau phase emission. We favor energy injection scenarios with a roughly linearly increasing input energy versus time for six well sampled events with nearly flat light curves at $t \approx 10^3 - 10^4$ s. Also, using the transition time T_H as the delineation between the GRB and afterglow emission, we calculate that the kinetic energy in the afterglow shock is typically a factor of 10 lower than that released in the GRB. Three very bright events suggest that this presents a missing X-ray flux problem rather than an efficiency problem for the conversion of kinetic energy into the GRB. Lack of hardness variations in these three events may be due to a very highly relativistic outflow or due to a very dense circumburst medium. There are a handful of rare cases of very late time $t > 10^4$ s hardness evolution, which may point to residual central engine activity at very late time.

¹Townes Fellow, Space Sciences Laboratory, University of California, Berkeley, CA, 94720-7450, USA

²Astronomy Department, University of California, 445 Campbell Hall, Berkeley, CA 94720-3411, USA

Subject headings: gamma rays: bursts — supernovae: general — X-rays: general

1. Introduction

The X-ray telescope (Burrows et al. 2005b) on *Swift* (Gehrels et al. 2004) is opening a new window into the early lives of γ -ray Bursts (GRBs) and their afterglows. Although hints and probable examples of highly time variable X-ray behavior at early time were seen prior to *Swift* (e.g., Piro et al. 2005; Watson et al. 2006), the XRT has shown us that this behavior is the norm. Nearly all afterglows show a period of rapid flux decline after the prompt or flare emission and about half show bright X-ray flares (e.g., Burrows et al. 2007). How these observations are to be reconciled with the well-tested internal/external shock GRB and afterglow model (Rees & Mészáros 1994; Sari & Piran 1997; Sari, Piran, & Narayan 1998; Wijers & Galama 1999) — which explained very well pre-*Swift* observations of simple fading powerlaws at late time — comprises a set of key open questions.

An accurate accounting of the GRB and afterglow phenomenology is critical for comparison to the models. O’Brien et al. (2006) have shown that the late GRB as measured by the Burst Alert Telescope (BAT) transitions in time smoothly into the early X-ray counts detected by the XRT, provided a correction is made for the different energy bands. This demonstrates a close connection between the early X-ray emission and that from the GRB. In Butler & Kocevski (2007, BK07), we fit the BAT and XRT spectra to explicitly show that the best-fit models at early time are those which fit GRB spectra well. The early X-ray spectra look like GRB spectra (but have νF_ν peak energies E_{peak} in the X-ray band rather than the γ -ray band) and evolve spectrally in a similar fashion (see, also, Falcone et al. 2006; Godet et al. 2007). Combined with studies in the time domain indicating fine timescale variability (e.g., Burrows et al. 2005a; Falcone et al. 2006; Romano et al. 2006; Pagani et al. 2006; Kocevski, Butler, & Bloom 2007), we are becoming confident that the X-ray emission prior to about 10^3 s is due to the GRB. The flat or “plateau phase” light curve which is typically present after this phase remains, however, largely mysterious.

Several models have been proposed to explain the plateau phase light curve. Because it is difficult to produce so flat a decay in the external shock picture, the energetics may be driven by a re-injection from the central engine or late time internal shocks (e.g., Nousek et al. 2006; Zhang et al. 2006; Ghisellini et al. 2007; Panaitescu et al. 2006; Panaitescu 2007). Off-axis external shocks (Eichler & Granot 2006), the reverse shock (Genet, Daigne, & Mochkovitch 2007; Uhm & Beloborodov 2007), or time-varying microphysical parameters (Granot & Kumar 2006) may also be responsible.

Observationally, Willingale et al. (2006) have shown that the prompt and afterglow emission can be separated near the start of the plateau by fitting two models (of the same form) to each inferred component. This split falls short of decisive because Willingale et al. (2006) are unable to measure the rise of the afterglow component from under the prompt component. The number of degrees of freedom in the model is large (6–8) and comparable to the typical number of powerlaw segments in broken powerlaw fits, which assume no separation into prompt and afterglow components. As we show below, a cleaner separation that requires no manual removal of flare-like emission is possible if we consider the spectral variations at early time. This can be demonstrated through the use of time resolved spectroscopy as discussed above, although such efforts are limited to bright events with high signal-to-noise. Because spectral fits are not required, variations in the X-ray hardness ratio provides an alternative. Studying the hardness ratio, we can link the plateau phase emission to late-time external shock emission for even faint bursts.

After a brief review of the X-ray phenomenology versus time gleaned from powerlaw fits (Section 3), we discuss in Section 4 how the hardness evolution implies a separation between prompt and afterglow emission. Stable hardness ratios during and after the plateau phase are exploited to constrain the GRB and afterglow models in Sections 5 and 6.

2. Data Reduction

We download the *Swift* XRT data from the *Swift* Archive¹. The data are processed with version 0.10.3 of the `xrtpipeline` reduction script from the HEASoft 6.0.6² software release. We employ the latest (2006-12-19) calibration files. The reduction of XRT data from cleaned event lists output by `xrtpipeline` to science ready light curves and spectra is described in detail in Butler & Kocevski (2007). Our final light curves have a fixed signal-to-noise of 3 in the 0.3–10.0 keV band.

We define an X-ray hardness ratio HR as the fraction of counts in the 1.3–10.0 keV band to the counts in the 0.3–1.3 keV band. On average, this ratio is equal to unity for XRT data. The mean energy index (flux proportional to $E^{-\beta}$) is $\beta = 1$ (Butler 2007a). We show in BK07 that the column densities N_H , as inferred from soft X-ray absorption, do not appear to change in time for *Swift* afterglows. To lowest order for a typical column density $N_H = 10^{21} \text{ cm}^{-2}$, $\beta \approx 1 - 0.9 \log_e(HR)$.

¹<ftp://legacy.gsfc.nasa.gov/swift/data>

²<http://heasarc.gsfc.nasa.gov/docs/software/lheasoft/>

2.1. Light Curve Region Selection and Fitting

To group the data into separate regions of similar temporal and spectral evolution, we fit the data using an extension of the Bayesian blocks algorithm (Scargle 1998) to piecewise logarithmic data. Our implementation is simple and requires no human intervention. Considering each data point as the location of a possible powerlaw break in the light curve, we calculate χ_ν^2 for every possible connection of the data points. This search can be done efficiently using publicly available Bayesian blocks code³. Because we also include an additional term (a prior against the break) with each possible new segment of $\Delta\chi_\nu^2 = 9.2$, each new segment must improve the fit at $\gtrsim 99\%$ confidence. The $\Delta\chi_\nu^2$ additions exclude models with many breaks, while the final fit without the $\Delta\chi_\nu^2$ contributions has $\chi_\nu^2 \approx \nu$ and typically 3–5 powerlaw segments.

So that noise fluctuations in the data do not generate spurious light curve breaks, we denoise the soft and hard channel light curve with Haar wavelets (see, Kolaczyk & Dixon 2000) prior to fitting. We fit the count rate and hardness simultaneously so that spectrally distinct regions are separated. The fits are plotted in red in the figures below. Light curves and fits for all *Swift* events can be downloaded from⁴.

3. Temporal/Spectral Overview of Swift and pre-Swift X-ray Afterglows

The X-ray spectral and temporal properties of GRB afterglows are typically garnered from powerlaw fits in time and energy. For *Swift* data, this can be done for individual events at multiple epochs. A detailed study of the evolution across all of these snapshots is beyond the scope of this paper, and we restrict our analysis in this section to the time regions as though they were separate events. It is reasonable to compare *Swift* data to pre-*Swift* data in this fashion, because pre-*Swift* fits correspond to a narrow time windows in the life of each afterglow and do not typically allow for time evolution studies for individual bursts. We determine fit regions with the blocking algorithm described above, and the results are binned in time into the three time epochs.

We show in BK07 that powerlaw energy fits are inappropriate at early time. This can also be seen in the first panel of Figure 1, which plots the energy index β versus the temporal index α for 59 *Swift* afterglows prior to and including GRB 070208 (see Table 1). For $t < 10^3$ s, there is a very wide range in β , consistent with the combined range of low-

³<http://space.mit.edu/CXC/analysis/SITAR/>

⁴<http://astro.berkeley.edu/~nat/swift>

energy and high-energy indices observed in *BATSE* GRBs (Preece et al. 2000; Kaneko et al. 2006). Nearly half of these points (42%) are inconsistent with any of the external shock synchrotron models plotted as diagonal lines. The fraction is greater than a half (52%) if we consider bursts separately, rather than plotting multiple spectra from individual events. We show in BK07 that the X-ray spectra are well fit by the same Band et al. (1993) model which fits the GRB spectra. The large scatter in the time indices for $t < 10^3$ s is due to rapid light curve decays and flaring. In Section 4 we show that the X-ray hardness can be used to infer the end of this phase.

From $10^3 \lesssim t \lesssim 10^4$ s, the X-ray light curves typically decay at a much slower rate. As shown in Figure 1 (middle panel), there is apparently little spectral evolution. Most of the fits (79%) and about half of the total number of bursts (53%) are consistent with an adiabatic shock observed above the cooling frequency ν_c . Willingale et al. (2006) also find that about half of all bursts are not consistent with this synchrotron model due to anomalously slow time decays. The fraction of consistent spectra is larger, because the events without plateaus are generally brighter at this stage. The plateau events can be modelled assuming a smooth re-injection of energy into the external shock at late time (Nousek et al. 2006; Zhang et al. 2006) or by deceleration of the external shock in a wind density ($n \propto R^{-2}$) external medium (Panaitescu 2007).

After 10^4 s, the fits exhibit a tight clustering in both α and β and 88% of the temporal/spectral snapshots (or 80% of bursts) are consistent with the behavior expected from an adiabatically expanding shock in the circumburst medium, emitting synchrotron radiation above the cooling frequency with electron index $p \approx 2$ (e.g., Sari, Piran, & Narayan 1998). The pre-*Swift* X-ray data from Beppo-SAX (see, e.g., de Pasquale et al. 2006) and Chandra and XMM (see, e.g., Gendre, Corsi, & Piro 2006) are all taken beginning after this time and show closely consistent behavior with the *Swift* events plotted here. Apparent here, but discussed in detail in Willingale et al. (2006) and Panaitescu (2007), few of these events here fit the expectation for a jetted afterglow (Rhoads 1999).

4. $T \sim 10^3$ s and the End of Hardness Variations

Figure 2 plots the X-ray hardness ratio versus time since the GRB trigger for the full sample of XRT afterglows. We also show ± 1 times the root-mean-square scatter in the data in red. The scatter is several times greater prior to 10^4 s than after. The reason for this scatter becomes clear when looking at the afterglows from individual bursts. Figure 3 shows the X-ray light curves and coincident X-ray hardness ratios for six events. Each shows an early period of strong hardness variation, which flattens out to a late-time value after several

hundred seconds. The hard, late-time component appears to overwhelm the soft, early-time component. We mark as the T_H the time at which the hardness reaches a minimum in each plot, before gradually increasing to a constant late-time value.

Figure 4 plots the distribution of end times of these hardness variations T_H for 50 afterglows (also Table 1). The flux prior to T_H is typically far softer than that after the start of the plateau phase, and the plateau phase becomes evident in HR plots prior to becoming evident in the 0.3–10.0 keV count rate. We note that the 0.3–10.0 keV light curves transition smoothly across T_H . Therefore the energy integrated light curve cannot be used to measure T_H . Several additional events, with and without flaring light curves, are plotted in BK07.

There is a significant anti-correlation between the time since the end of the BAT emission $T_H - T_{90}$ and the X-ray flux at T_H (Kendall’s $\tau_K = -0.46$, signif.= 2×10^{-6}), which reflects the decay of the GRB flux and its intersection at T_H with a range of possible flux levels for the afterglow plateau phase component.

The end times T_H are on average 5 ± 3 longer than the prompt T_{90} durations. The X-ray flux at T_H is on average $10^{1.9 \pm 0.8}$ times fainter than the average flux for the GRB measured in BAT. These quantities are only weakly correlated: T_{90} versus T_H has a Kendall’s $\tau_K = 0.20$, signif.= 0.04 and F_X versus F_γ has a Kendall’s $\tau_K = 0.03$, signif.= 0.71.

We can use the light curve taxonomy developed by other authors to relate our times T_H to the “canonical” (e.g., Nousek et al. 2006) light curve decay phases. O’Brien et al. (2006) and Willingale et al. (2006) divide the light curves into prompt and afterglow phases by fitting models to the energy integrated light curves. These authors estimate durations which represent the brightest and most slowly decaying time regions, excluding the rapidly time-decaying tails of the emission episodes. Our T_H values are on average ten times longer than the prompt time T_P in Willingale et al. (2006), but there is no significant correlation ($\tau_K = -0.04$, signif.= 0.75, for $N = 35$ bursts). There is also no significant correlation between T_H and the Willingale et al. (2006) T_A ($\tau_K = 0.1$, signif.= 0.43, for $N = 35$), which approximately measures the end of the plateau phase and is on average twenty times larger than our T_H .

Given T_H as a dividing line between emission with strikingly different temporal and spectral characteristics — which we can interpret as a dividing line in time between GRB and afterglow emission — it is possible to separate and compare the fluence from the GRB and afterglow. Figure 5 plots the fluence prior to T_H versus the fluence after T_H . The afterglow emits an amount of energy proportional to ($\tau_K = 0.35$, signif.= 3×10^{-4}) and $10^{1.0 \pm 0.5}$ times lower than the GRB. The fluence in the X-ray band prior to T_H contributes only 10% additional fluence, on average, to the GRB as observed in BAT. These quantities

are possibly weakly correlated ($\tau_K = 0.18$, signif. = 0.07). The prompt and afterglow fluences we find here are consistent with those reported by Willingale et al. (2006, Fig 3) using two-component model fits to the light curves, but our fluences correlate with less scatter (Figure 5).

5. Achromaticity of the X-ray Plateau Phase at $10^3 \lesssim T \lesssim 10^4$ s

The events selected for plotting in Figure 3 have prominent flat X-ray light curves at $10^3 \lesssim t \lesssim 10^4$ s. On the *HR* panel for each burst in Figure 3 we print the maximal *HR* variation between data points after 10^3 s. This is always less than 0.5, corresponding to $\delta\beta < 0.5$. $\delta\beta = 0.5$ is the expectation for changes due to cooling in the external shock (e.g., Sari, Piran, & Narayan 1998; Chevalier & Li 2000). If we place a tighter constraint on the allowed hardness ratio variations by allowing only powerlaw increases or decreases after 10^3 s, then the limits on $\delta\beta$ are much tighter, $\delta\beta \lesssim 0.1$. We thus see no evidence for significant spectral evolution in these events after 10^3 s.

We also observe no significant variation in β from powerlaw fits, consistent with the *HR* analysis. Combining this information to derive a constant β in time for each event, we can plot α and β across the break (Figure 6). Many of the light curve breaks in Figure 3 are gradual and are fit here with multiple powerlaw segments. As seen in Figure 6 and discussed more below, the values of (α, β) during the plateau are consistent with values produced in energy injection models. As the light curve breaks, the (α, β) approach those expected from external shock models without energy injection.

6. Discussion

We have exploited an autonomous spectral/temporal division of early afterglow data to isolate the time when models for the GRB afterglows well-tested prior to the launch of *Swift* first begin to match the data well. From powerlaw fits in time and energy (Section 3), the afterglow models appear to break down strongly prior to $t \lesssim 10^4$ s. This is consistent with the findings of O’Brien et al. (2006); Willingale et al. (2006). We focus here on rapid time variations in the X-ray hardness, which end by $T_H \approx 10^2 - 10^4$ s and therefore allow for a clean separation of early, GRB-like emission and later afterglow-like emission without hardness variations.

Our finding here that the end time of hardness variations T_H anti-correlates strongly with the X-ray flux at T_H (Figure 4) likely has a trivial explanation: because the light curve

is decreasing logarithmically after T_{90} , the length of the duration $T_H - T_{90}$ simply reflects the faintness of the afterglow. More interesting, the large dynamic range in this correlation between prompt and afterglow fluences (Figure 5) indicates that some physical feature of the explosion or circumburst cite must be able to substantially modulate the fraction of energy in highly relativistic material (the GRB) or the shock kinetic energy (the X-ray afterglow).

GRB models must be able to explain how the fireball deceleration (see, Mészáros 2002, and references therein) can be postponed until after $t \approx 10^3$ s — and probably until after $t \approx 10^4$ s — when the afterglow light curve is no longer flat or rising. There must be no apparent imprint of the external medium on the light curve or spectrum prior to $t \approx 10^3$ s. Because the deceleration time $t_{\text{dec}} = 390(1+z)E_{\text{shock},53}^{1/3}n_1^{-1/3}\Gamma_2^{-8/3}$ s (e.g., Piran 1999; Ramirez-Ruiz, Merloni, & Rees 2001), this might be accomplished by increasing in the shock kinetic energy $E_{\text{shock},53}$ [10^{53} erg] via energy injection, by having a very low density n [cm^{-3}], or by placing much of the outflow in low Lorentz factor $\Gamma = 100 \Gamma_2$ material. The importance of these parameters becomes more apparent if we focus on extreme cases (Sections 6.1 and 6.2) or on modelling of the more typical cases (Section 6.3).

6.1. Events with No Hardness Variations

There was an expectation, based primarily on detections of putative afterglow components in the tails of GRBs (Connaughton 2002; Giblin et al. 2002; Lazzati, Ramirez-Ruiz, & Ghisellini 2001) and also from studies extrapolating the X-ray afterglow flux back to the prompt emission (e.g., Costa et al. 1997; Piro et al. 1998; Frontera et al. 2000), that the X-ray afterglows measured by *Swift* would directly proceed and connect to the prompt emission. That is, the emission at $t \approx 10^2 - 10^4$ s was expected to mirror the temporal/spectral properties of the well-established later emission plotted in the third panel of Figure 1. Instead, the rapid time-variation and plateau phases generally occur, with strong spectral variations during the rapid time-variation phase. It is a well known fact that the late-time emission in *Swift* GRB X-ray afterglows does not typically extrapolate back in time to the end of the prompt emission (e.g., Nousek et al. 2006; Zhang et al. 2006; O’Brien et al. 2006; Willingale et al. 2006). Instead, the X-ray light curve is relatively flat prior to $t \approx 10^4$ s, and this results in typical X-ray fluences that are ten times lower than the GRB fluence (Figure 5, also, Zhang et al. 2006b; Granot & Kumar 2006). Because the late time X-ray emission is typically argued to trace the kinetic energy explosion (Kumar 2000; Freedman & Waxmann 2001), this may lead to an efficiency problem because the shock energy available to the GRB is very low (e.g., Piran 1999).

Because efficiency of the conversion of shock kinetic energy to the energy released by

the GRB is an intrinsic property, we would expect that the efficiency should vary little from event to event and that all events should exhibit an X-ray plateau. However, there are few bursts — <10% of the 30 or so afterglow observations which began early and measured with high signal-to-noise the tail of the prompt emission — which do not show early HR variation and do appear to show an afterglow-like component decaying as a powerlaw after the prompt emission at $t \gtrsim 100$ s. The best example GRBs 050717 (also, Krimm et al. 2006), 060105 (also, Tashiro et al. 2006), and 061007 (also, Mundell et al. 2007; Schady et al. 2007) are shown in Figure 8. These have especially bright and hard prompt emission with $E_{\text{peak}} \gtrsim 500$ keV (suggestive of high Γ) and hard X-ray emission detected beginning after $t \approx 90$ s with energy index $\beta \approx 1$. Perhaps an early deceleration occurs for these events due to an anomalously high circumburst density. Could these events also be telling us that energy is present but not observed in the soft X-ray band in the other, more common afterglows with prominent plateau phases? Where is this energy?

One possibility is the two jet model (Eichler & Granot 2006), with a GRB jet containing more kinetic energy per solid angle than in the afterglow. Panaitescu (2007) has tested and found no evidence for this scenario. Another possibility is that the early forward shock emission is suppressed as it scatters (to the GeV-TeV range) photons from the late-time internal shocks and flares (Wang, Li, & Mészáros 2006). Understanding a possible energy removal mechanism and its impact on the fluence correlation (Figure 5) will likely help also to understand a possible correlation between the end of the plateau phase and the GRB energy reported in O’Brien et al. (2006) and Nava et al. (2007).

Finally, we note that GRBs 050717, 060105, and 061007 may be representative of a separate class of GRBs to which previous missions were more sensitive. This would explain why afterglow-like tails are rarely observed just following *Swift* GRBs. In part, previous mission were likely also less sensitive to the very soft emission detected by *Swift*. A handful of these — 050502B, 050724, 061222B, 070129 — have very soft emission between T_{90} and T_H which is greater than the prompt fluence. These events may help us to understand how X-ray Flashes (Heise et al. 2000) are related to GRBs. A late and bright X-ray flare as in 050502B likely produced the soft X-ray excess in the enigmatic GRB 031203 (Watson et al. 2006).

6.2. Events with Very Late-time Hardness Variations, The External Shock?

There are rare events which show hardness variations with $\Delta HR > 0.5$ after $t \approx 10^3$ s (Figure 7), which is probably too late for an explanation involving the deceleration of the GRB fireball. The unusual supernova-GRB 060218 stops varying in hardness just after 10^4 s.

(Given the extremely long prompt duration of this event ($T_{90} \approx 2 \times 10^3$ s; Sakamoto et al. 2006), the late hardness evolution may not be unusual. This GRB and afterglow produces a clear arc from $t \approx 300 - 3000$ s in Figure 2, which demonstrates a HR values and evolution distinct from those observed in any other event.) The high- z GRB 050904 light curve appears to consist entirely of flares, and this is reflected in late-time hardness variations.

The hardness increases at late-time for GRB 060206 (the outlier in Figure 4). The additional cases (GRBs 050315, 060105, 060814) show a decreasing hardness on a timescale similar to the observations time. The hardness variation is consistent with the factor of two expected from the $\Delta\beta = 0.5$ change expected from a cooling break in the synchrotron shock picture (e.g., Sari, Piran, & Narayan 1998; Chevalier & Li 2000). Although we believe we have accounted for the flux of a nearby source, it is possible that the hardness increase in the case of GRB 060206 is due to contamination by that source. This is not an issue for GRBs 050315, 060105, and 060814.

For GRB 060206 at $z = 4.045$ (Fynbo et al. 2006), the source-frame GRB energy release is $E_{\text{iso}} = 4.2_{-0.6}^{+0.8} \times 10^{52}$ erg. The break to increased hardness in Figure 7 for a wind medium implies a reasonable density $A_* = 0.13(\epsilon_B/0.01)^{-3/4}$. If the density were uniform, as would be inferred from the breaks to softer spectra in the other 3 events, a very low density $n = 1.7 \times 10^{-5}(\epsilon_B/0.01)^{-3/2}$ is implied. Unless the other 3 events are at low redshift ($z \lesssim 0.1$), which is unlikely given the lack of bright optical emission in each case, the implied densities are anomalously low.

Falling back on our basic ignorance of the nature of the prompt engine and its timescales for energy output, the late time variation could also be due to the central engine. The light curves do appear more structured than simple powerlaws. In Figure 7, we fit the observed 0.3–10 keV rate model to the HR in order to derive a hardness intensity correlation index. These are printed in the figure and are typically ≈ 0.5 for the early, GRB-like emission and ≈ 0 for the late emission. As we discuss in BK07, a probable explanation for this correlation at early times is a relativistic viewing effect due to photon arrival from emitting regions off the line of site. The long emission timescales could be due to curvature radiation at large radii. It is interesting to note that the late hardness evolution in GRB 050315 rules out associating the late break with an achromatic jet break, as was done in Vaughan et al. (2006).

6.3. Energy Injection Scenarios

The lack of spectral evolution during the light curve plateau phase and at later time suggests strongly that these episodes are generated by the same emission mechanism. In the fireball model, this points to a smooth late-time energy injection that refreshes the external shock (Nousek et al. 2006; Zhang et al. 2006), which alters only the time decay rate and not the spectral regime in which the X-ray synchrotron emission occurs. The external shock without energy injection cannot produce the observed flat light curves (e.g., Sari, Piran, & Narayan 1998).

Energy injection into the GRB external shock was first discussed by Paczyński (1998) and Rees & Mészáros (1998). According to the very general energy injection models outlined in Nousek et al. (2006), the X-ray light curve is propped up by an insertion of energy E in time as $E \propto t^a$. For data observed above the synchrotron cooling break ν_c and peak frequency ν_m , the flux varies as $F_X \propto t^{-\alpha_{\text{inj}}}$, with $\alpha_{\text{inj}} = \alpha - a(\beta + 1)/2 = (3 - a)\beta/2 - (1 + a)/2$. Curves for a in the range 0.5–1.1 — which is needed to account for the well-sampled plateau phase events described in Section 5 — are shown in Figure 6. Time flows from the left to the right in this figure as the light curve smoothly breaks. We consider the left-most points for each burst as those most likely to reflect the true energy injection profile. If the X-ray band is below the cooling break, the slopes in Figure 6 remain the same for the same a but the offsets shift. This leads to acceptable fits with $a = 0.7 - 1.1$ for a constant density (ISM) medium and $a = 1.0 - 1.4$ for a wind density medium. An $E \propto t$ scaling implies a central engine with an approximately constant late-time luminosity or an ordered flow of internal shock material with $M(> \Gamma) \propto \Gamma^{-2} - \Gamma^{-5}$ (ISM medium) reaching the afterglow shock at late time (Nousek et al. 2006; Granot & Kumar 2006).

After the break, the fits become consistent with external shock models ranging between the expectation for a spherical expansion observed at $\nu > \nu_c, \nu_m$ and a jetted expansion in the same regime. This may imply that gradual jet breaks are present in these events, although only one (060614) ever reaches the expected late-time decay rate.

Alternatively, the X-ray band could be in the $\nu_c > \nu > \nu_m$ regime and the energy injection could be turning off gradually. The steep decay in the case of 060614 at late time requires a wind density medium. However, this can be ruled out from optical data reported to the GCN⁵. During the plateau, the optical light curve rise as $t^{0.38 \pm 0.06}$, as compared to $t^{-0.03 \pm 0.05}$ measured in the X-ray band. This behavior is consistent with ν_c between the optical and X-ray band and energy injection with $a = 0.69 \pm 0.08$. There are no optical

⁵<http://gcn.gsfc.nasa.gov>

points after the candidate jet break to verify achromaticity. GRB 060729 has consistent optical ($t^{-0.24\pm 0.03}$) and X-ray ($t^{-0.26\pm 0.04}$) light curve indices during the plateau, and both light curves break to consistent decays thereafter. The post break decay is consistent with expansion into an ISM medium without a jet break. The energy injection prior to the break is fit by $a = 0.92 \pm 0.05$ ($\nu > \nu_c, \nu_m$).

Panaitescu (2007) propose a very simple model to explain some plateau light curves and spectra. For a wind density medium, t_{dec} is a strong function of the bulk Lorentz factor, $t_{\text{dec}} = 6(1+z)E_{\text{shock},53}A_*^{-1}\Gamma_2^{-4}$ s for a typical Wolf-Rayet wind density of $5 \times 10^{11}A_* \text{ g cm}^{-1}$. The afterglow will not peak until $10^3 - 10^4$ s if, after the internal shocks are through, the effective $\Gamma \sim 20$. During deceleration, the flow coasts and the light curve stays relatively flat, $\alpha = \beta - 1$ (Panaitescu 2007), for $\nu > \nu_c, \nu_m$. Contrarily, deceleration by a uniform density medium produces a sharply rising light curve, which is not observed. This α, β relation for the wind medium takes the same form as that for the $a = 1$ energy injection model, and it appears to be roughly consistent with most of the plateaus in Figure 6. In this picture, the jet break will coincide with the end of the plateau if the opening angle is $\theta \approx 1/\Gamma \approx 3^\circ$, which may well occur for some events.

Several additional models have been proposed to explain the X-ray plateau phase, and many of these can be constrained by a constant X-ray spectral slope and from the fact that a distinct hardness evolution separates the plateau phase emission from the GRB-like emission prior. One possibility — which we can rule from lack of hardness variations because it requires contribution from the spectrally varying tail of the GRB — is that off-axis afterglow plus late GRB emission combine to produce the plateau (Eichler & Granot 2006). In a similar fashion, we may be able to rule out the “late prompt” model of Ghisellini et al. (2007), although spectral variations would be modest in that model due to low Γ . Models involving the reverse shock (Genet, Daigne, & Mochkovitch 2007; Uhm & Beloborodov 2007) appear to produce spectra variations in the X-ray band. Inverse Compton models which extract afterglow flux should also change the spectrum, but see Wang, Li, & Mészáros (2006). A final, more exotic possibility which we cannot rule out is time evolution of the microphysical parameters defining the shock (Granot & Kumar 2006).

7. Conclusions

We have shown that GRB and early afterglow light curve prior to $T_H \sim 10^3$ s is highly time and energy variable. The flux at the end of these variations and during the X-ray plateau phase exhibits non-changing X-ray hardness like the latest X-ray afterglow emission that is well modelled by a synchrotron external shock ($t \gtrsim 10^4$ s; Section 3). The afterglow

flux is typically ten times lower than would be estimated from a simple extrapolation of the GRB flux after $T_{90} \sim T_H/5$. Explaining how the GRB deceleration can be postponed until after $t \gtrsim 10^4$ s is a central challenge to those modelling GRB and their afterglows.

Observations prior to *Swift* which imply a common early onset of the afterglow may point to a class of bursts rarely observed by *Swift*. The three *Swift* examples discussed (GRBs 050717, 060105, and 061007) have energetic and hard prompt emission. These bursts may be those most rapidly decelerated by the circumburst medium. These events likely have the most high energy photons for *GLAST* to observe, unless photons missing from the early afterglows of softer events are preferentially up-scattered to high energies by late time shocking (see, e.g., Wang, Li, & Mészáros 2006). In either cases, *GLAST* observations will be crucial for understanding this diversity and for helping us to understand the *Swift* phenomenology relative to that observed in previous missions (see, e.g., Zhang 2007). Additional long wavelength observations (e.g., in the optical/IR) are also essential at times $t \lesssim 10^3$ s, because these better probe the circumburst density structure.

N. R. B gratefully acknowledges support from a Townes Fellowship at U. C. Berkeley Space Sciences Laboratory and partial support from J. Bloom and A. Filippenko. D. K. acknowledges financial support through the NSF Astronomy & Astrophysics Postdoctoral Fellowships under award AST-0502502. Special thanks to the *Swift* team for impressively rapid public release and analysis of the XRT data. Thanks to J. Bloom and the U. C. Berkeley GRB team for comments on the manuscript and several useful conversations. We thank an anonymous referee for a very useful and critical reading of the manuscript.

REFERENCES

- Band, D. L., et al. 1993, ApJ, 413, 281
- Barthelmy, S. D., et al. 2005, Nature, 438, 994
- Berger, E., Kulkarni, S. R., & Frail, D. A. 2003, ApJ, 590, 379
- Borgonovo, L, & Ryde, F. 2001, ApJ, 548, 770
- Burrows, D. N., et al. 2005a, Science, 309, 1833
- Burrows, D. N., et al. 2005b, Space Sci. Rev., 120, 165
- Burrows, D. N., et al. 2007, Philosophical Transactions A. Accepted, astro-ph/0701046

- Butler, N. R. 2007a, ApJ, 656, 1001
- Butler, N. R. 2007b, AJ, 133, 1027
- Butler, N. R., & Kocevski, D. 2007, ApJ Accepted, astro-ph/0612564 (BK07)
- Campana, S., et al. 2006, Nature, 442, 1008
- Campana, S., et al. 2006b, GCN #5162
- Campana, S., et al. 2006c, ApJL Accepted, astro-ph/0611305
- Chevalier, R. A., & Li, Z.-Y. 2000, ApJ, 536, 195
- Connaughton, V. 2002, ApJ, 567, 1028
- Costa, E., et al. 1997, Nature, 387, 783
- Cusumano, G., et al. 2006, Nature, 440, 164
- Dickey, J. M., & Lockman, F. J. 1990 ARAA, 28, 215
- Fan, Y. Z., & Wei D. M. 2005, MNRAS, 364, L42
- Falcone, A., et al. 2006, ApJ, 641, 1010
- Fenimore, E. E., et al. 1995, ApJ, 448, L101
- Fenimore, E. E., Madras, C. D., & Hayakshin, S. 1996, ApJ, 473, 998
- Peng, F., Konigl, A., & Granot, J. 2005, ApJ, 626, 966
- Fishman, G. J., et al. 1989, in Proc. GRO Science Workshop (Greenbelt: NASA GSFC), 2-39
- Ford, L. A., et al. 1995, ApJ, 439, 307
- Freedman, D. L., & Waxmann, E. 2001, ApJ, 547, 922
- Frontera, F., et al. 2000, ApJ, 127, 59
- Fynbo, J. P. U., et al. 2006, A&A, 451, 47
- Eichler, D. & Granot J. 2006 ApJ, 641, L5
- Gehrels, N., et al. 2004, ApJ, 611, 1005

- Gehrels, N., et al. 2006, GCN #5839
- Gendre, B., Corsi, A., & Piro L. 2006, A&A, 455, 803
- Genet, F., Daigne, F., & Mochkovitch, R. 2007, MNRAS Submitted, astro-ph/0701204
- Ghisellini, G., et al. 2007, ApJsubmitted, astro-ph/0701430
- Giblin, T. W., et al. 2002, ApJ, 570, 573
- Godet, O., et al. 2007, A&ASubmitted, astro-ph/0702262
- Golenetskii, S. V., et al. 1983, Nature, 306, 451
- Granot, J., & Kumar, P. 2006, MNRAS, 366, L13
- Granot, J., Konigl, A., & Piran, T. 2006, MNRAS 370, 1946
- Granot, J., Piran, T., & Sari, R. 1999, ApJ, 513, 679
- Grupe, D., et al. 2006a, GCN #5365
- Grupe, D., et al. 2006b, GCN #5505
- Heise, J., et al. 2000, in Proc. 2nd Rome Workshop: Gamma-ray Bursts in the Afterglow Era, eds. E. Costa, F. Frontera, J. Hjorth (Berlin: Springer-Verlag), 16
- Holland, S. T., et al. 2006, GCN #4570
- Ioka, K., et al. 2005, ApJ, 631, 429
- Kaneko, Y., et al. 2006, ApJS, 166, 298
- Kargatis, V. E., et al. 1995, Ap&SS 231, 177
- Kocevski, D., Ryde, F., & Liang, E. 2003, ApJ, 596, 389
- Kocevski, D., Butler, N. R. 2007, & Bloom, J. S, Submitted to ApJ, astro-ph/0702452
- Kocevski, D., et al. 2007, in preparation
- Kolaczyk, E. D., Dixon, D. D. 2000, ApJ, 534, 490K
- Krimm, H. A., et al. 2006, ApJ, 648, 1117
- Kumar, P. 2000, ApJ, 538, L125

- Kumar, P., & Panaitescu, A. 2000, *ApJ*, 541, L51
- Lazzati, D., Ramirez-Ruiz, E., & Ghisellini, G. 2001, *A&A*, 379, L39
- Lazzati, D., & Perna, R., *MNRAS* in press, astro-ph/0617030
- Lazzati, D., & Begelman, M. C. 2006, *ApJ*, 641, 972L
- Liang, E., & Kargatis, V. 1996, *Nature*, 381, 49
- Liang, E. W., et al. 2006, *ApJ*, 646, 351
- O’Brien, D. P., et al. 2006, *ApJ*, 647, 1230
- Markwardt, C. B., et al. 2006, *GCN #5654*
- Mészáros, P. 2002, *ARA&A*, 40, 137
- Morreti, A., et al. 2006, *A&A*, 451, 777
- Mundell, C. G., et al. 2007, *ApJAccepted*, astro-ph/0610660
- Nava, L., et al. 2007, *MNRAS Submitted*, astro-ph/0701705
- Norris, J. P., et al. 1996, *ApJ*, 459, 393
- Norris, J. P., 2002, *ApJ*, 579, 386
- Nousek, J. A., et al. 2006, *ApJ*, 642, 389
- Pagani, C., et al. 2006, *ApJ*, 645, 1315
- Page, K. L., et al. 2006, *GCN #5823*
- de Pasquale, M., et al. 2006, *A&A*, 455,8 13
- Paczynski, B. 1998, *ApJ*, 494, L23
- Painetescu, A., et al. 2006, *MNRAS*, 366, 1357
- Painetescu, A. 2007, *MNRAS submitted*, astro-ph/0612170
- Parsons, A. M., et al. 2006, *GCN #5252*
- Piran, T. 1999, *Physics Reports*, 314, 575
- Piro, L., et al. 1998, *A&A*, 331, L41

- Piro, L., et al. 2005, *ApJ*, 623, 314
- Preece, R. D., et al. 2000, *ApJ*, 126, 19S
- Protassov, R., et al. 2002, *ApJ*, 571, 545
- Ramirez-Ruiz, E., Merloni, A, & Rees, M. J. 2001, *MNRAS*, 324, 1147
- Qin, Y.-P., et al. 2004, *ApJ*, 617, 439
- Qin, Y.-P., & Lu, R. J. 2005, *MNRAS*, 362, 1085
- Rees, M. J., & Mészáros, P. 1994, *ApJ*, 430, L93
- Rees, M. J., & Mészáros, P. 1998, *ApJ*, 496, L1
- Rhoads, J. 1999, *ApJ*, 525, 737
- Rol, E., et al. 2006, *MNRAS Accepted*, astro-ph/0611554
- Romano, P., et al. 2006, *A&A*, 450, 59
- Ryde, F., & Petrosian, V. 2002, *ApJ*, 578, 290
- Ryde, F. 2005, *A&A*, 429, 869
- Sakamoto, T., et al. 2003, *ApJ*, 602, 875
- Sakamoto, T., et al. 2006, *GCN #4822*
- Sari, P., & Piran, T. 1997, *ApJ*, 485, 270
- Sari, R., Piran, T., & Narayan, R. 1998, *ApJ*, 497, L17
- Sari, P., Piran, T., & Halpern J. P. 1999, *ApJ*, 519, L17
- Scargle, J. D. 1998, *ApJ*, 504, 405S
- Schady, P., et al. 2007, *MNRAS Submitted*, astro-ph/0611081
- Shen, R. F., Song, L. M., & Li, Z. 2005, *MNRAS*, 362, 59
- Starling, R. L. C., et al. 2005, *A&A*, 442, 21
- Tagliaferri, G., et al. 2005, *Nature*, 436, 985
- Tashiro, M. S., et al. 2006, *PASJ Accepted*, astro-ph/0609437

- Uhm, Z. L. & Beloborodov, A. M. 2007, ApJSubmitted, astro-ph/0701205
- Vaughan, S., et al. 2006, ApJ, 638, 920
- Watson, D., et al. 2006, ApJ, 636, 967
- Willingale, R., et al. 2006, astro-ph/0612031
- Wijers, R. A. M. J., & Galama, T. J. 1999, ApJ, 523, 177
- Woods, E., & Loeb, A. 1999, ApJ, 523, 187
- Yamazaki, R., et al. 2006, MNRAS, 369, 311
- Zhang, B., et al. 2006, ApJ, 642, 354
- Zhang, B., et al. 2006b, ApJSubmitted, astro-ph/0610177
- Zhang, B. 2007, ChJAA, 7, 1-50
- Zhang, B.-B., Liang, E. W., & Zhang, B. 2006, astro-ph/0612246
- Wang, X.-Y., Li, Z., & Mészáros, P. 2006, ApJ, 641, L89

Table 1: X-ray Hardness Evolution End Times T_H

GRB	T_H [s]	GRB	T_H [s]	GRB	T_H [s]	GRB	T_H [s]
050219A	165^{+35}_{-35}	050315	221^{+100}_{-100}	050502B	974^{+82}_{-82}	050607	410 ± 40
050712	428^{+59}_{-59}	050713A	203^{+31}_{-31}	050714B	400^{+4300}_{-20}	050716	544^{+170}_{-170}
050721	1135^{+242}_{-242}	050724	323^{+38}_{-38}	050730	779^{+11}_{-11}	050801	737^{+142}_{-142}
050814	562^{+275}_{-274}	050820A	4750^{+100}_{-100}	050822	600^{+32}_{-32}	050922B	1121^{+129}_{-129}
051117A	1659^{+54}_{-54}	051227	220 ± 100	060115	594^{+152}_{-152}	060204B	378^{+37}_{-37}
060206	21284^{+15275}_{-15275}	060210	426^{+7}_{-7}	060211A	391^{+88}_{-87}	060312	176^{+29}_{-29}
060418	175^{+12}_{-12}	060427	226^{+26}_{-26}	060428A	95^{+8}_{-8}	060428B	271^{+35}_{-35}
060510B	415^{+21}_{-21}	060526	374^{+16}_{-16}	060604	193^{+4}_{-4}	060607A	289^{+7}_{-7}
060614	2588^{+2127}_{-2127}	060707	6300^{+565}_{-565}	060708	88^{+11}_{-11}	060714	232^{+12}_{-12}
060719	255^{+147}_{-147}	060729	271^{+26}_{-26}	060904A	413^{+47}_{-47}	060904B	1948^{+1652}_{-1652}
060929	630^{+11}_{-11}	061110A	390^{+26}_{-26}	061121	142^{+11}_{-11}	061202	390^{+199}_{-199}
061222A	203^{+18}_{-18}	061222B	275^{+48}_{-48}	070107	477^{+29}_{-29}	070110	254^{+100}_{-101}
070129	948^{+171}_{-171}	070208	2585^{+2175}_{-2175}				
Limits							
050401	<153	050416A	<126	051016B	<91	051109A	<195
060111B	<145	060211B	<95	060219	<158	060502A	<88
060510A	<110	060906	<276	060908	<90		

Notes: Several afterglows allow for only a T_H limit measurement.

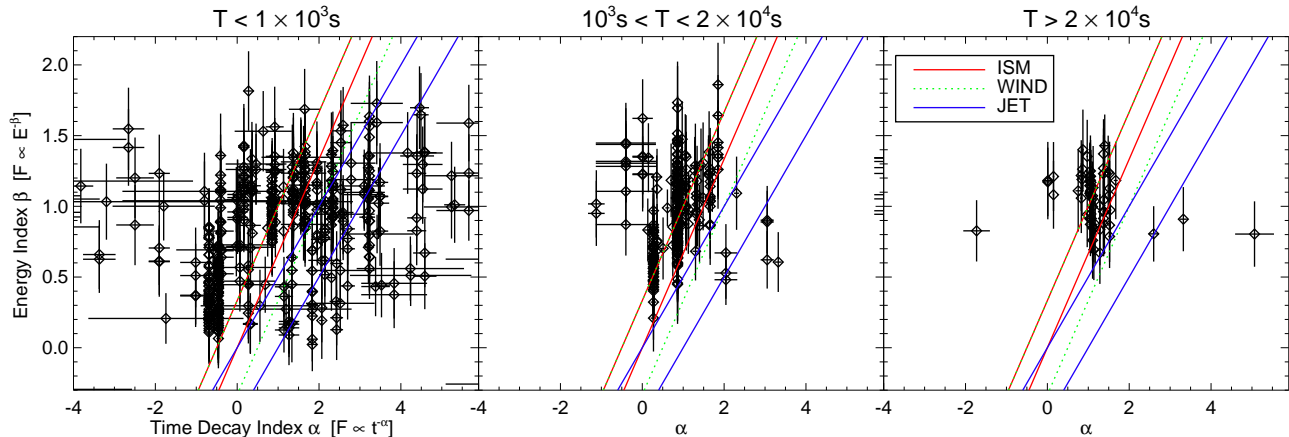


Fig. 1.— Powerlaw energy index versus powerlaw light curve index for the X-ray afterglows at 3-time epochs after the GRB. The solid curves show the expected “closure relations” for an adiabatic expanding external shock emitting synchrotron radiation (Sari, Piran, & Narayan 1998; Chevalier & Li 2000; Sari, Piran, & Halpern 1999). Only after $t = 2 \times 10^4$ s — a time corresponding to all pre-*Swift* X-ray afterglow observations — are the data overwhelmingly consistent with the models.

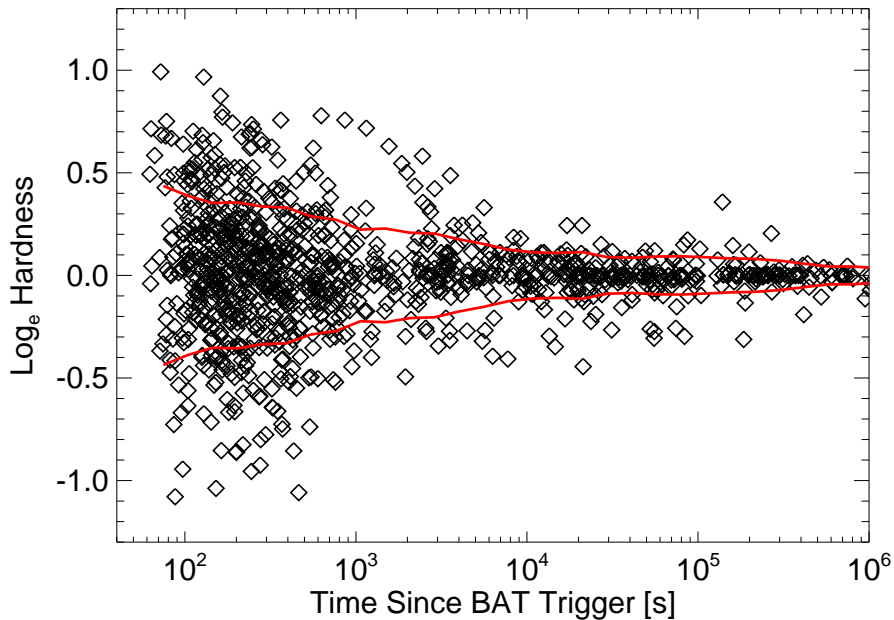


Fig. 2.— The scatter in hardness ratio for the full *Swift* sample prior to GRB 070208 drops rapidly with observation time since the GRB trigger. We have subtracted off a constant HR from each burst, which we obtain by fitting the data at $t > 10^4$ s.

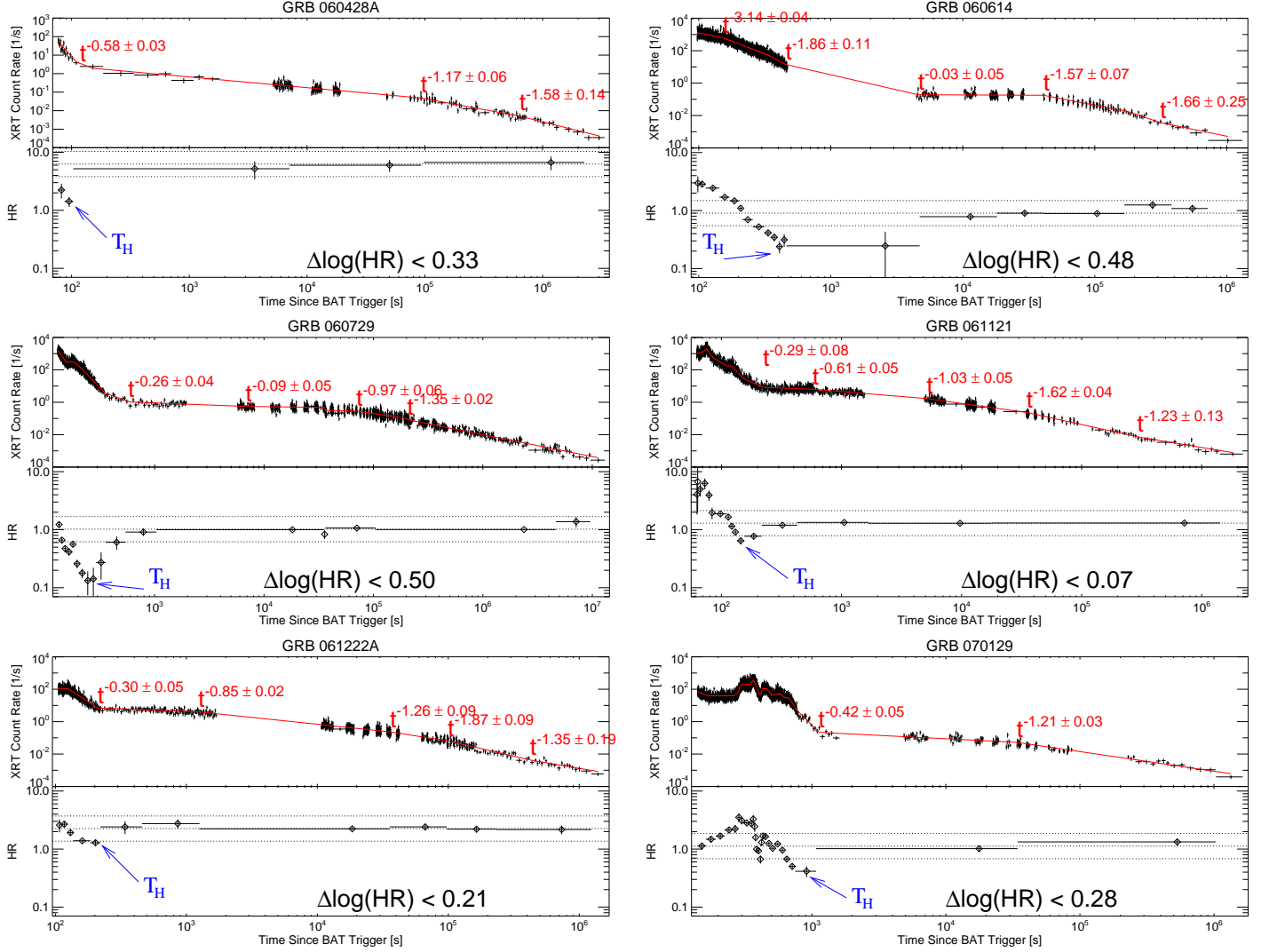


Fig. 3.— X-ray Light curve and hardness ratio HR plots for several GRB afterglows with prominent light curve “plateau” phases. The temporal indices of the best fit temporal powerlaw models (red curves) for the counts rates are shown. T_H marks the end of an early phase of strong hardness evolution in each case. At later time, HR is consistent with constant. The dotted lines mark the best-fit late-time value as well as $e^{0.5}$ and $e^{-0.5}$ times the best-fit value, as a characteristic expected range for variations in external shock synchrotron models. A limit on the maximum deviation (1-sigma) from the best-fit late-time HR value is also given.

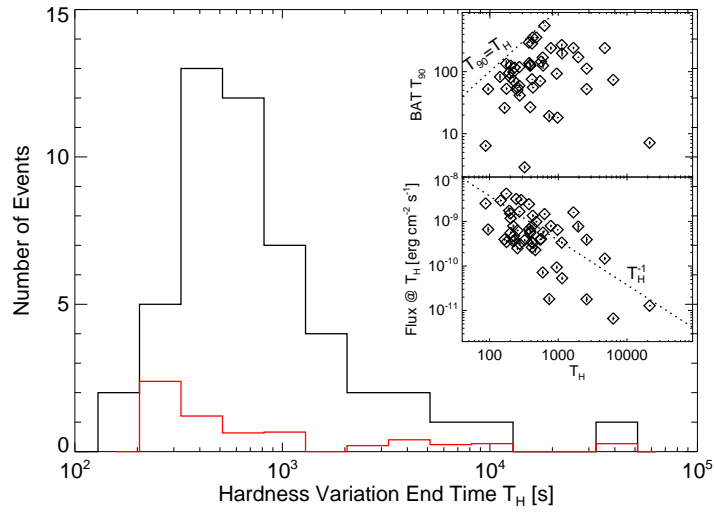


Fig. 4.— Frequency distribution (black histogram) of the latest time at which spectral hardness variations are observed T_H (Table 1) for 50 events. The hardness typically remains constant after this time (Figure 3). The red histogram for fewer events is divided through by the event redshift $(1+z)$. The subpanel shows the T_{90} duration measured in BAT versus the hardness variation end-time and also the X-ray flux at T_H versus T_H . There is a weak correlation with T_{90} and a strong correlation with F_X . On average, T_H is 5 times greater than T_{90} and the X-ray flux at T_H is 175 times below the average GRB flux observed by BAT.

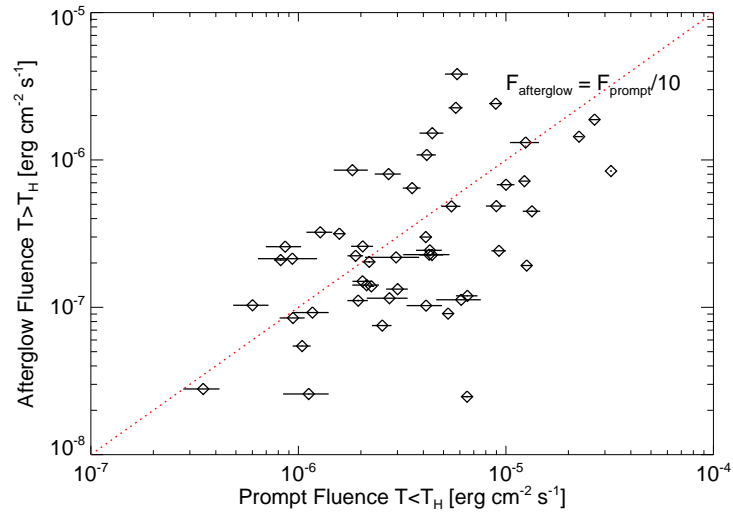


Fig. 5.— Time integrated flux before T_H compared to after T_H . The fluence in the afterglows ($T > T_H$) component is on average ten times less than the fluence in the prompt GRB and early X-ray emission.

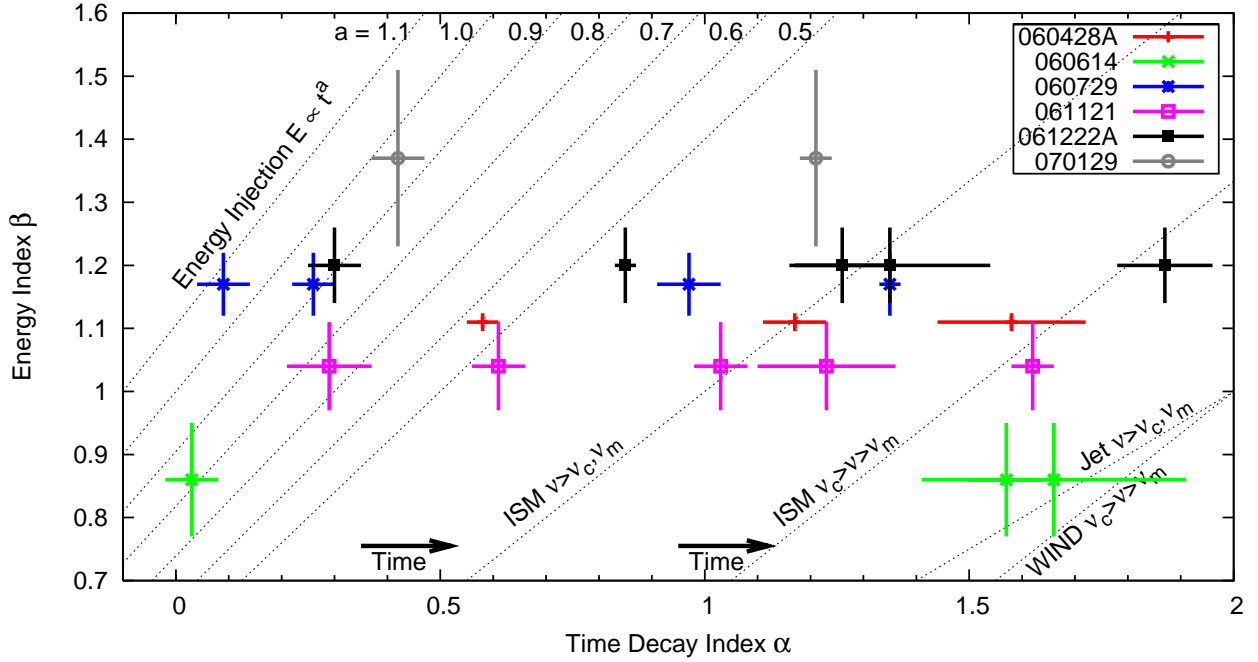


Fig. 6.— Energy and time indices for powerlaw segments in the six bright plateau events from Figure 3. Separate events are color coded. Indices for the flat, plateau phase of the light curve in each case are consistent with energy injection models (dotted lines shown are for $\nu > \nu_c, \nu_m$). The break in time to a steeper fade — which occurs roughly after the model marked $a = 0.5$ in this plot — is gradual. The powerlaw indices at late time approach those expected from the external shock models. Models for the late time emission of spherical and jetted shocks are plotted.

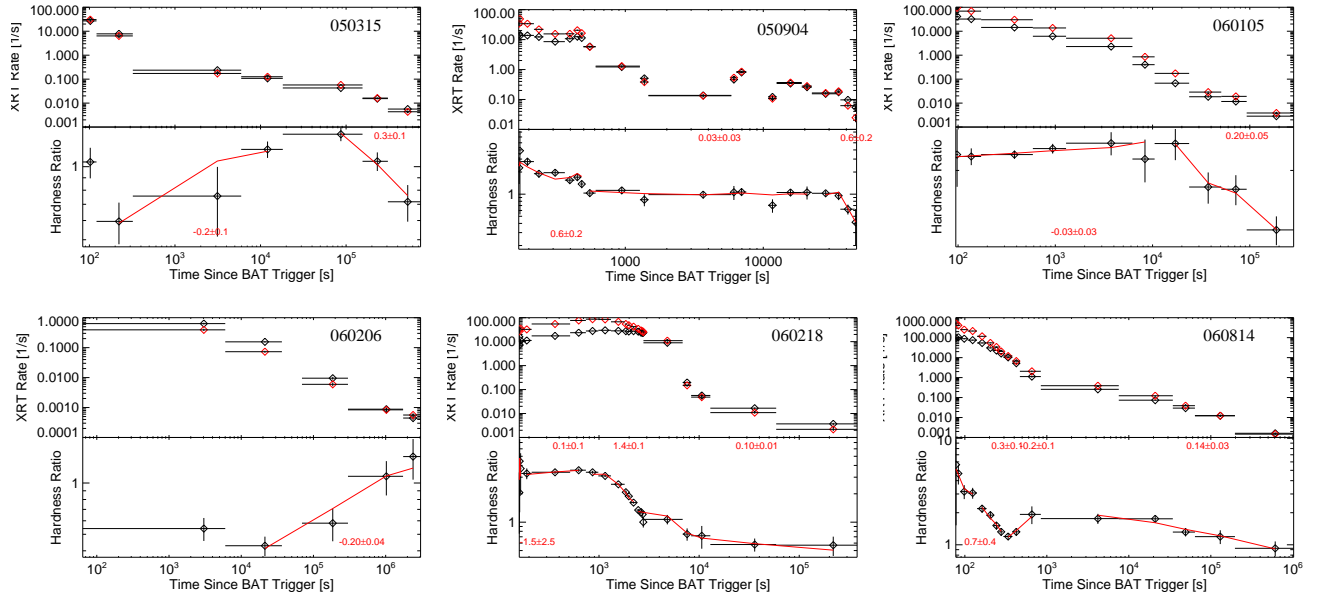


Fig. 7.— X-ray Light curve and hardness ratio HR plots for rare GRB afterglows which show late-time hardness variations. These variations may imply very late time central engine activity. Fits of the observed flux to HR are plotted in red, and index values ≈ 0.5 are expected for internal shocks (Butler & Kocevski 2007).

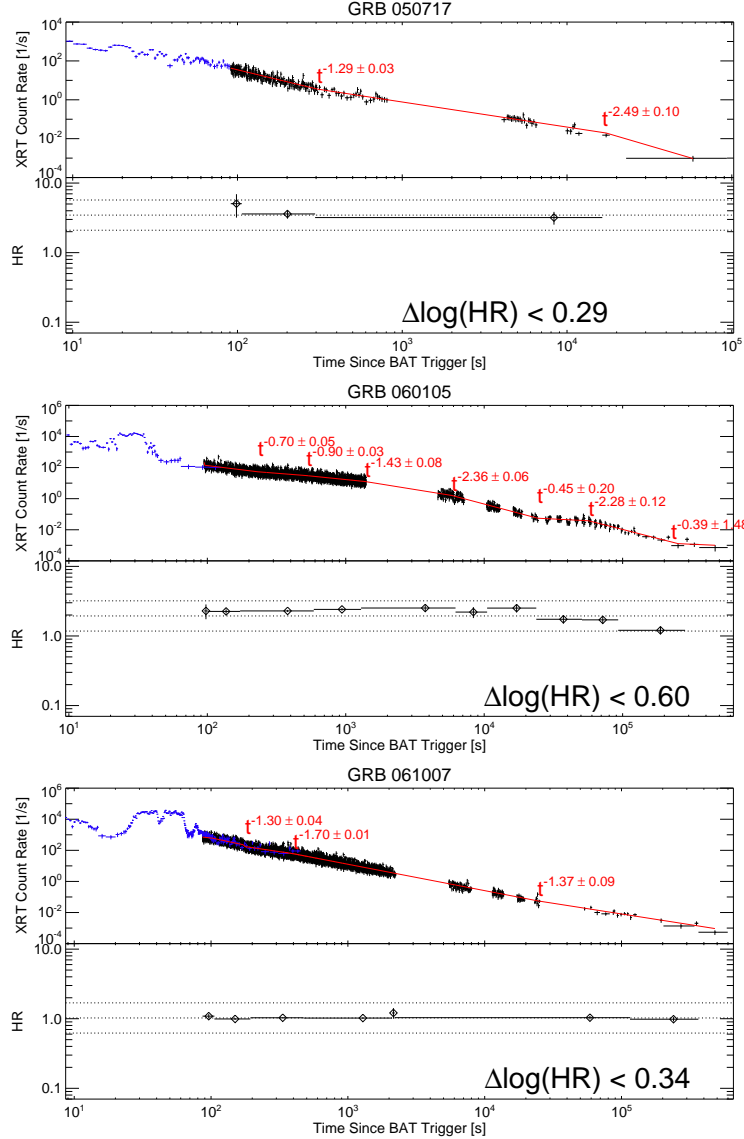


Fig. 8.— X-ray Light curve and hardness ratio HR plots for three events where the GRB tail (blue points) connects directly with a powerlaw (afterglow-like) X-ray light curve exhibiting little spectral variation. The X-ray data in these cases are well fit by powerlaws with energy index $\beta = 1.0 \pm 0.1$ throughout. The dotted lines mark an expected range for variations in external shock synchrotron models (also Figure 3). In the case of GRB 060105, the 1-sigma limit on $\Delta \log(HR) \propto \Delta\beta/0.9$ is consistent with a possible cooling break at $t \approx 10^4$ s.